Dalton Transactions

PAPER

View Article Online
View Journal | View Issue



Cite this: *Dalton Trans.*, 2015, **44**, 20685

# A trigonal prismatic $Cu_6$-pyrazolato complex containing a $\mu_6$-F ligand†

Logesh Mathivathanan,[a] Karrar Al-Ameed,‡[b] Katerina Lazarou,[c] Zdeněk Trávníček,[d] Yiannis Sanakis,[c] Radovan Herchel,*[d] John E. McGrady*[b] and Raphael G. Raptis*[a]

Received 6th October 2015,
Accepted 30th October 2015

DOI: 10.1039/c5dt03892h

www.rsc.org/dalton

The encapsulation of a fluoride ion in a trigonal prismatic $Cu^{II}_6$-pyrazolato cage results in a small expansion of the $Cu_6$-host. The structural, electronic and magnetic features of the $Cu_6$-complex, containing an endohedral fluoride in the rare $\mu_6$-F coordination mode, are compared with those of the parent complex with a vacant $Cu_6$-cage.

## Introduction

Structural changes in multinuclear complexes of open-shell metals are reflected in their intramolecular isotropic Heisenberg exchange parameters ($J$), whose sign and magnitude are related to the topology of the magnetically coupled cluster. Simple magnetostructural relationships exist for several dinuclear and trinuclear systems with a single (or one predominant) magnetic exchange path. Among such complexes, those of $M_2(\mu\text{-O/OR})$ and $M_3(\mu_3\text{-O/OR})$, M = Cu and Fe, are the best studied.[1–4] Even subtle structural changes, such as the M–O–M angle, are often clearly reflected in the magnitude of $J$ values, determined by analysis of the solid state, variable temperature, magnetic susceptibility measurements.[5] However, in larger clusters, simple magnetostructural relationships are often less easy to define, and *a priori* prediction of the magnetic properties remains a challenge.[6] As part of our ongoing work exploring the chemistry of new molecular architectures based on trinuclear Cu(II)-pyrazolato triangles, we have reported the structures, electrochemistry and magnetochemistry of hexanuclear trigonal prismatic $Cu_6$-pyrazolato complexes of the general formula $[PPN][\{Cu_3(\mu_3\text{-O})(\mu\text{-4-R-pz})_3\}_2(3,5\text{-Ph}_2\text{-4-R'-pz})_3]$, ($Cu_6$-cages, [PPN][**1**], R = R′ = H, [PPN] = bis(triphenylphospine)iminium cation).[7] Magnetic susceptibility studies of [PPN][**1**] showed a spin-frustrated system with a stronger antiferromagnetic isotropic exchange within the triangular $Cu_3(\mu_3\text{-O})$-units and a weaker one between them.[8] We have also shown that [PPN][**1**] and its analogues (R, R′ = Cl) undergo two reversible one-electron electrochemical oxidations to mixed-valent $Cu^{II/III}$ species.

Here we describe a related homovalent Cu(II)$_6$–pyrazolate cluster, $[\{Cu_3(\mu_3\text{-OH})(\mu\text{-pz})_3\}_2(\mu\text{-3,5-Ph}_2\text{pz})_3(\mu_6\text{-F})]$, **2**, now containing an encapsulated $\mu_6$-fluoride ion, isolated in the course of our efforts to prepare the aforementioned chemically oxidized variants of [PPN][**1**] with $[Fc][PF_6]$ as an oxidizing agent. Fluoride ions typically form complexes with the alkali and alkaline earth metals where the coordination numbers are generally high,[9] but complexes with the coinage metals are less common.[10] Whilst encapsulated halide ions have recent precedent, Cu–F bonds are in general uncommon; fluorides have often been used to stabilize higher oxidation states of Cu such as $Cu^{III}$ as in the paramagnetic $K_3CuF_6$ [10a] and $Cu^{II}$–F and $Cu^{III}$–F bonds have also been proposed as intermediates in aryl fluorinating reagents.[10b] Fluoride coordination to trinuclear Cu-complexes also has some biological relevance as even concentrations of $F^-$ as low as $10^{-6}$ to $10^{-4}$ M can inhibit the electron transfer chemistry of laccase-like enzymes.[11] The original serendipitous synthesis of **2** was subsequently reproduced systematically, and we report here its X-ray crystal structure and magnetic properties along with a comparison of its electronic structure to [PPN][**1**].

## Results and discussion

Ferricinium hexafluorophosphate, $[Fc][PF_6]$, is a convenient one-electron oxidant, especially for sequential oxidations, and we have used it extensively in the course of studies of redox-active clusters. However, the inadvertent generation of $F^-$ from

[a]*Department of Chemistry and Biochemistry, Florida International University, 11200 SW 8th ST, Miami, FL, USA, 33199. E-mail: rraptis@fiu.edu*
[b]*Department of Chemistry, South Parks Road, University of Oxford, OX1 3QR, UK. E-mail: john.mcgrady@chem.ox.ac.uk*
[c]*Institute of Nanoscience and Nanotechnology, NCSR "Demokritos", 15310 Ag. Paraskevi, Attiki, Greece*
[d]*Regional Centre of Advanced Technologies and Materials, Department of Inorganic Chemistry, Faculty of Science, Palacký University, 17. listopadu 12, CZ-77146 Olomouc, Czech Republic. E-mail: radovan.herchel@upol.cz*

†Electronic supplementary information (ESI) available: Fit of the magnetic data of **2** without antisymmetric exchange and total energies and optimised cartesian coordinates for all computed spin states. CCDC 1429538. For ESI and crystallographic data in CIF or other electronic format see DOI: 10.1039/c5dt03892h

‡Permanent address: Faculty of Science, University of Kufa, Najaf, Iraq.

the hydrolysis of $[PF_6]^-$ is a known phenomenon when humidity is not vigorously excluded, and hydrolysis products of $[PF_6]^-$ in the presence of $Ag^+$ have been reported in the literature.[12] In fact, controlled decomposition of $[BF_4]^-$ or $[PF_6]^-$ has been used systematically to prepare transition metal fluoride complexes.[13] A variant of [Fc][$PF_6$] has been found to hydrolyze into $F^-$ and phosphate, forming a metal–organometallic framework (MOMF) that contains a $Co_{12}(\mu_3\text{-F})$-cage. Attempts to prepare the MOMF with deliberate addition of $H_3PO_4$ and HF were not successful.[14] A similar fluoride abstraction under oxidizing conditions leads here to a new $Cu_6$-pyrazolato complex containing novel ($\mu_6$-F). The nature of the $\mu_6$-ion was probed quantitatively by elemental analysis of the bulk product.

Complex **2** was crystallized – by layering MeCN, hexane, or toluene over a $CH_2Cl_2$ solution – in the triclinic $P\bar{1}$ space group with the whole molecule in the asymmetric unit (Fig. 1) and crystallographically disordered MeCN solvent molecules, which were removed by the SQUEEZE program of the PLATON suite. Selected bond lengths of [PPN][**1**], along with the corresponding distances of similar [$Cu_6(\mu_6\text{-Cl})$] and [$Cu_6(\mu_6\text{-CF})$]-complexes, are listed in Table 1.

The hexanuclear core of complex **2** is very similar to that of the anion $[\mathbf{1}]^-$, consisting of two triangular $Cu_3(\mu\text{-pz})_3$-units, clipped together by three μ-3,5-$Ph_2$-pz bridges which hold the two $Cu_3$-units in a trigonal prism. The trigonal prismatic arrangement of $Cu_3$-triangles is uncommon in Cu–pyrazolate chemistry, and only three examples are available in the literature, reported by us[7,8] and by others.[15–17] The capping ($\mu_3$-OH) ligands of **2** are located 0.824 and 0.858 Å above the $Cu_3$-planes, a somewhat larger deviation than found in typical $Cu_3(\mu_3\text{-OH})$ complexes where the capping-OH is located only *ca.* 0.50 Å above the plane.[18] Complex **2** contains an unsymmetrically encapsulated $\mu_6$-F ion with Cu–F distances in the range 2.383(5)–2.605(5) Å and the fluoride ligand located 1.610 and 1.693 Å from the two $Cu_3$-planes, forming Cu–F–Cu angles of 81.3(1)°–83.7(1)°. In related [$Cu_3(\mu_3\text{-X})_2$]-complexes (X = Cl and Br) the $\mu_3$-X ligands are again located farther from the $Cu_3$-plane, forming similarly acute Cu–X–Cu angles ($Cu_3$-plane···$\mu_3$-X: 1.769 Å and 1.927 Å for X = Cl and Br, respectively; Cu–X–Cu: ~80°).[18,19] The Cu···F distances are significantly longer than the sums of copper and fluorine ionic radii (1.98 Å) and covalent radii (2.09 Å), but shorter than the sum of their van der Waals radii (2.87 Å). No single radius can capture the size of a highly anisotropic ion like $Cu^{2+}$: in this case the fluoride ligand is directed towards the doubly occupied $d_{z^2}$, so the van der Waals radius gives the most faithful estimate of the size of the cavity required to accommodate the fluoride ion. In the [$Cu_6(\mu_6\text{-F})$] complex reported by Cañon-Mancisidor *et al.*, [$Cu_6(\mu_6\text{-F})(\mu\text{-OH})(\mu_3\text{-OCH}_3)_2(\mu\text{-OCH}_3)_2$(3,5-$Me_2$pz)$_6$], has two pyrazolate and one methoxy "clips" between $Cu_3$-units, making both the Cu···Cu and Cu–F bonds shorter than those of **2** (see Table 1). The structural parameters of **2** are also comparable to those previously reported for the corresponding [$Cu_6(\mu_6\text{-Cl}]$ complex in which the $\mu_6$-Cl is equidistant from both $Cu_3$-planes at 1.829 Å. Similar Cu–Cl distances are also present in a related [$Cu_6(\mu_6\text{-Cl})$]-complex where the $Cu_3$-triangles are connected only by the $\mu_6$-Cl ligand, as a result of which the Cu centres are much farther apart (4.21 Å).[20] Comparison of the structure with that of PPN[**1**] shows that the endohedral $F^-$ brings about only minor structural changes to the $Cu_6$-cage, although the trigonal prismatic cavity expands to accommodate the fluoride ion in **2**. In PPN[**1**] the planarity of $Cu_3(\mu_3\text{-O})$ triangles imposes a strained geometry on the four-coordinate Cu-centres with *trans* O–Cu–N angles of 156.6(2)°–168.6(2)°. In contrast, the pyramidal $Cu_3(\mu_3\text{-OH})$ moieties in **2** allow a relaxed coordination sphere with *trans* HO–Cu–N angles approximating the ideal 180°.

**Table 1** Important interatomic distances in Å

| | $Cu_6F$, **2** | $Cu_6Cl$[a] | $Cu_6F$[b] | $Cu_6$, PPN[**1**] |
|---|---|---|---|---|
| Cu···Cu (inter-trimer) | 3.281(2), 3.335(2), 3.289(2) | 3.621, 3.675 | 3.056–3.382 | 2.975, 2.999, 3.028 |
| Cu···Cu (intra-trimer) | 3.234(2)–3.289(2) | 3.209, 3.233 | 2.832–3.112 | 3.206–3.279 |
| Cu···X | 2.383(5)–2.605(5) (X = F) | 2.603, 2.623 (X = Cl) | 2.338, 2.344, 2.420 (X = F) | N/A |
| Cu···($\mu_3$-OR) | 2.048(3)–2.096(5) (R = H) | 2.083, 2.084 (R = Me) | 1.984, 1.991, 2.012, 2.013 (R = Me) | 1.883–1.894 |

[a] From ref. 15. [b] From ref. 17.

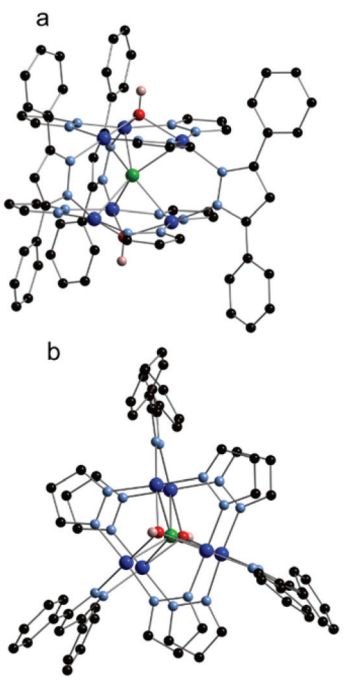


**Fig. 1** Molecular structure of **2**. (a) Side view and (b) top view. Carbonic H atoms are not shown. Color coding: Cu, blue; O, red; N, light blue, C, black; H, pink; and F, green.

### Analysis of the magnetic data

The temperature dependence of effective magnetic moment and the isothermal magnetization data for the reported compound **2** are depicted in Fig. 2. The effective magnetic moment is 3.67$\mu_B$ at room temperature, decreasing almost linearly to 2.36$\mu_B$ at 50 K and finally dropping sharply to 0.64$\mu_B$ at 1.9 K. The 50 K value of 2.36$\mu_B$ is much lower than the theoretical spin only value for six non-interacting Cu(II) ions with $g$ = 2.0 (4.24$\mu_B$), indicating the existence of strong antiferromagnetic exchange interactions. The observed behaviour of $\mu_{eff}/\mu_B$ can be rationalized on a qualitative level by assuming dominant antiferromagnetic exchange within each $\mu_3$-OH–$Cu_3$ triangle, which leads to $S_{Cu_3}$ = 1/2 ground spin states. The two doublet states then couple weakly through pyrazolate ligands to generate a singlet and triplet: in the limit of weak coupling two independent $S$ = 1/2 paramagnets yield a $\mu_{eff}$ of 2.45$\mu_B$ for $g$ = 2.0, close to the experimental value at 50 K.

A more quantitative analysis comes from considering the spin Hamiltonian shown in eqn (1), which is precisely analogous to that used in the analysis of $[\mathbf{1}]^-$.

$$\begin{aligned}\hat{H} = &-J_1(\mathbf{S}_1\cdot\mathbf{S}_2+\mathbf{S}_2\cdot\mathbf{S}_3+\mathbf{S}_1\cdot\mathbf{S}_3+\mathbf{S}_4\cdot\mathbf{S}_5+\mathbf{S}_5\cdot\mathbf{S}_6+\mathbf{S}_4\cdot\mathbf{S}_6)\\ &-J_2(\mathbf{S}_1\cdot\mathbf{S}_4+\mathbf{S}_2\cdot\mathbf{S}_5+\mathbf{S}_3\cdot\mathbf{S}_6)+\mu_B g\sum_{i=1}^{6}\mathbf{B}\cdot\mathbf{S}_i\\ &+d_{12}\cdot(\mathbf{S}_1\times\mathbf{S}_2)+d_{23}\cdot(\mathbf{S}_2\times\mathbf{S}_3)+d_{31}\cdot(\mathbf{S}_3\times\mathbf{S}_1)\\ &+d_{45}\cdot(\mathbf{S}_4\times\mathbf{S}_5)+d_{56}\cdot(\mathbf{S}_5\times\mathbf{S}_6)+d_{64}\cdot(\mathbf{S}_6\times\mathbf{S}_4)\end{aligned} \quad (1)$$

$J_1$ and $J_2$ describe the isotropic exchange within $\mu_3$-OH–$Cu_3$ triangles and between the two triangles (mediated by pyrazolate ligands), respectively. Antisymmetric exchange within each $\mu_3$-OH–$Cu_3$ triangle was shown to be important in [**1**] and is expressed by $\mathbf{d}_{ij}$ vectors, $(d_x, d_y, d_z)_{ij}$.[21] Application of Moriya symmetry rules[22] for the triangle results in only one non-zero component: $\mathbf{d}_{ij}$ = (0, 0, $d_z$)$_{ij}$ and it was assumed that $(d_z)_{ij}$ are equal for all pairs. Furthermore, the averaged molar magnetization was calculated as an integral average (eqn (2)), because the measurement was performed on a powder sample (eqn (2))

$$M_{mol} = 1/4\pi\int_0^{2\pi}\int_0^{\pi} M_{mol}(\theta,\phi)\sin\theta \mathrm{d}\theta\mathrm{d}\phi \quad (2)$$

where the magnetic field vector is defined in the polar coordinates as

$$\vec{B} = B(\sin\theta\cos\phi, \sin\theta\sin\phi, \cos\theta)$$

The temperature- and field-dependent magnetic data were fitted simultaneously to the Hamiltonian (1), resulted in best-fit values of $J_1$ = −147 cm$^{-1}$, $J_2$ = −35 cm$^{-1}$, $|d_z|$ = 30.2 cm$^{-1}$ with an isotropic $g$-factor fixed to 2.1 (as used for $[\mathbf{1}]^-$). A small amount of monomeric paramagnetic impurity (PI) was introduced (mole fraction $x_{PI}$ = 2.7%), leading to a correction of the overall magnetization according to $M_{sample} = (1 - x_{PI})M_{mol} + 6{\cdot}x_{PI}{\cdot}M_{PI}$, where $M_{PI}$ was calculated using the Brillouin function. The fitted $J$ values are comparable to the constants reported by Kamiyama: ($Cu_6Cl$, $J_1$ = −133 cm$^{-1}$, $J_2$ = −34 cm$^{-1}$) and Coronado ($Cu_6F$ $J_1$(a) = −94 cm$^{-1}$, $J_1$(b) = −131 cm$^{-1}$, $J_2$(a) = −22 cm$^{-1}$ and $J_2$(b) = −4 cm$^{-1}$ where $J$-values have been scaled according to definition in eqn (1). A comparison of the fitted parameters of **2** with those previously reported for $[\mathbf{1}]^-$ ($J_1$(av) = −675 cm$^{-1}$, $J_2$ = −26 cm$^{-1}$, $g$ = 1.95 and $|d_z|$ = 30.0 cm$^{-1}$),[8] suggests that intra-triangular coupling is significantly reduced in **2**, while the inter-triangular coupling and the antisymmetric exchange parameters are very similar. Attempts to fit the magnetic data of **2** without the antisymmetric exchange, as done in $Cu_6Cl$[15] and $Cu_6F$,[17] resulted in $J_1$ = −151 cm$^{-1}$, $J_2$ = −47 cm$^{-1}$, $x_{PI}$ = 4.2% (Fig. S1, ESI†) and a rather larger deviation of the fit from the magnetic data, particularly at low temperature. On this basis, it seems that non-Heisenberg interactions may play a role in determining the magnetic behavior of **2**.

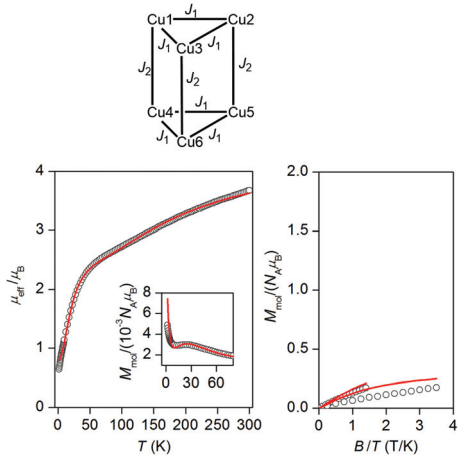


Fig. 2 Top: Scheme of spin Hamiltonian interaction used for magnetic analysis of **2**. Bottom: The magnetic data for **2**, the temperature dependence of the effective magnetic moment and molar magnetization measured at $B$ = 0.1 T; the reduced isothermal magnetization.

### EPR spectroscopy

The magnetic susceptibility measurements of **2** indicate antiferromagnetic interactions, which result in a diamagnetic ground state. At 4.2 K, the X-band EPR spectrum from a powdered sample of **2** gives rise to a weak signal, which is consistent with a monomeric $Cu^{2+}$ ($S$ = 1/2) species, most probably arising from impurities. At higher temperatures a new signal emerges at $g \sim 2.05$ (Fig. 3), whose temperature dependence indicates that it arises from excited states with $S \neq 0$. The spectra across the whole temperature range consist of a derivative-like Lorrentzian signal with a linewidth, $\Delta H_{pp}$, of ~400 G. No notable temperature-dependent shift in the resonance field or in linewidth is observed. The line-shape of the spectrum does not allow to identify contributions of sub-spectra attributable to distinct spin manifolds. The derivative-like signal is isotropic, apparently inconsistent with the antisymmetric exchange that proved significant in the fitting of the magnetic data. We suggest that at a given temperature the observed spectrum represents a thermal distribution over several spin states,

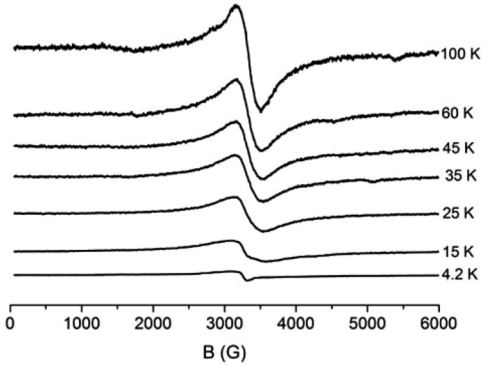


Fig. 3 X-band EPR spectra from a powdered sample of **2**. The spectra have been scaled as $I \times T$. EPR conditions: microwave power, 1.5 mW, modulation amplitude, 15 Gpp, microwave frequency, 9.42 GHz.

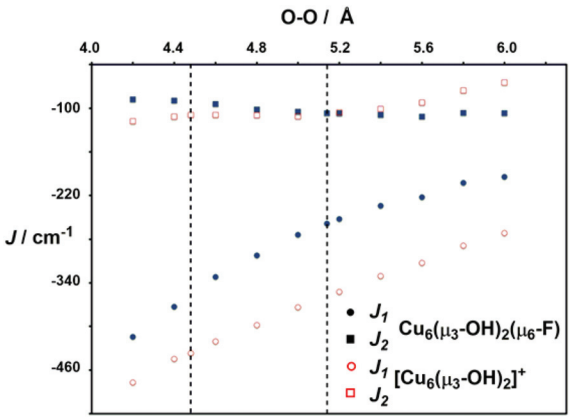


Fig. 4 Magnetostructural correlation showing the dependence of $J_1$ and $J_2$ on the separation between the two O centres for **2**, and the corresponding species where the fluoride ion has been removed. Vertical lines show the optimized O–O separations with (5.14 Å) and without (4.48 Å) fluoride ion.

averaging out any anisotropic effect. Similar isotropic signals have been observed in copper containing clusters and they have been interpreted on the basis of fast transition between different spin manifolds.[23]

### Computational analysis

In order to explore the nature of the magnetic interactions in **2**, we have performed a series of computations using broken-symmetry density functional theory, following the protocol developed in our previous paper on the $\mu_3$-O bridged $Cu_6$ cluster, $[\{Cu_3(\mu_3\text{-}O)(\mu\text{-}4\text{-}R\text{-}pz)_3\}_2(3,5\text{-}Ph_2\text{-}4\text{-}R'\text{-}pz)_3)]^-$ ($[\mathbf{1}]^-$). All calculations were performed using the B3LYP functional in the ADF2013 software package (see Computational methods for further details). In order to extract the coupling constants, $J$, differences in energy between various configurations are mapped onto differences between the diagonal elements of a Heisenberg spin Hamiltonian of the form

$$\hat{H} = -J_1(\mathbf{S}_1\cdot\mathbf{S}_2 + \mathbf{S}_2\cdot\mathbf{S}_3 + \mathbf{S}_1\cdot\mathbf{S}_3 + \mathbf{S}_4\cdot\mathbf{S}_5 + \mathbf{S}_5\cdot\mathbf{S}_6 + \mathbf{S}_4\cdot\mathbf{S}_6) - J_2(\mathbf{S}_1\cdot\mathbf{S}_4 + \mathbf{S}_2\cdot\mathbf{S}_5 + \mathbf{S}_3\cdot\mathbf{S}_6)$$

using the pairwise protocol proposed by Ruiz *et al.* The resulting values of $J_1$ and $J_2$ are $-130$ cm$^{-1}$ and $-51$ cm$^{-1}$, respectively, entirely consistent with the values of $-151$ cm$^{-1}$ and $-47$ cm$^{-1}$ obtained from the best fits to the experimental data. In comparison, the $\mu_3$-O analogue $[\mathbf{1}]^-$ studied previously has a very similar value of $J_2$ but more strongly antiferromagnetic $J_1$ (calculated: $J_1$ = –390 cm$^{-1}$ $J_2$ = –40 cm$^{-1}$ *vs.* measured $J_1$ = ~ $-630$ cm$^{-1}$ $J_2$ = –44 cm$^{-1}$, respectively.§ The reduction in the intra-triangle coupling, $J_1$, is typical of a switch from a $\mu_3$-O architecture with approximately planar $Cu_3O$ units to a highly pyramidalised $Cu_3(\mu_3\text{-}OH)$. In contrast the inter-triangle coupling, $J_2$, is largely unaffected by the change in $\mu_3$ bridging ligand. The presence of the $\mu_6$-F ligand is unlikely to provide effective exchange pathways for inter-triangle coupling as the Cu–F vectors are almost orthogonal to the magnetic orbitals (Cu $d_{x^2-y^2}$ in a local coordinate system), and indeed removing the fluoride (without allowing any structural relaxation) in fact alters the magnitude of both $J_1$ ($-146$ cm$^{-1}$) and $J_2$ ($-71$ cm$^{-1}$). However, when the cluster is allowed to relax after removal of the fluoride ion, the separation between the OH oxygen atoms decreases to 4.48 Å from a value of 5.14 Å in **2** (dashed lines in Fig. 4): the steric pressure exerted by the fluoride effectively inflates the cluster, pushing the $\mu_3$-OH ligand out of the $Cu_3$ plane.

In both **2** and the corresponding cation where the fluoride has been removed, the values of $J_1$ are strongly dependent on the O–O separation: shorter distances allow the $Cu_3(\mu_3\text{-}OH)$ units to approach planarity more closely, and so maximise the overlap of the magnetic orbitals with the hydroxy bridge. The contraction of the O–O distance in the absence of fluoride causes a further indirect increase in $J_1$ to $-220$ cm$^{-1}$. Thus the presence of the fluoride clearly distorts the structure substantially, with the consequence that the magnetic exchange within the triangles is reduced.

## Conclusions

In this paper we report the synthesis and characterisation of a trigonal prismatic $Cu_6$ cluster containing an encapsulated $\mu_6$-$F^-$ ligand. The original observation of this cluster arose from serendipitous hydrolysis of a $[PF_6]^-$ anion, but it was subsequently synthesised *via* a rational route. The pre-formed $Cu_6$-cage acts as a host for the fluoride ion; fluoride is not a template for the organization of the $Cu_6$-cage around it. Structural characterization and a detailed analysis of the magnetic properties suggest that the fluoride ion inflates the $Cu_6$ cage, and the resultant greater pyramidalisation of the $Cu_3(\mu_3\text{-}OH)$ triangles causes a significant reduction in the intra-triangle coupling.

§ The value for $J_1$ is somewhat smaller than that reported in our previous work on $\mathbf{1}^+$,[8] where Gaussian basis sets were used.

# Experimental section

## Materials and methods

All reagents were purchased from commercial sources and used without further purification. Solvents were dried according to standard procedures. PPN[**1**] was prepared according to published procedure. Elemental analysis was performed at Galbraith Laboratories, Inc. $^1$H-NMR was recorded in $CD_2Cl_2$ in a Bruker Avance 400 spectrometer.

## X-ray crystallography

Single crystal X-ray crystallography data (Table 2) were obtained from a crystal mounted atop a glass fiber using a Bruker SMART APEX II diffractometer fitted with a graphite-monochromated Mo-Kα radiation at ambient temperature. Data were collected using the APEX 2 suite and corrected for Lorentz and polarization effects.[24] The structure was refined using the SHELXTL-direct methods and refined by full-matrix least squares on $F^2$.[25] The disordered interstitial water electron densities were removed by employing the SQUEEZE procedure supplied with the PLATON suite.[26] CCDC reference number 1429538.

## Magnetic measurements

The temperature dependence of the magnetization at an applied field of $B$ = 0.1 T and the field dependence of the magnetization up to $B$ = 7 T at $T$ = 2 and 5 K were acquired for a powder sample of **2** using MPMS XL7 SQUID magnetometer (Quantum Design). The experimental data were corrected for the underlying diamagnetism using empirical equation, $\chi_{dia} = -5M \times 10^{-12}$ m$^3$ mol$^{-1}$ (SI units), where $M$ is molar mass of the compound in g mol$^{-1}$.[27]

Table 2 Crystallographic data for **2**

| | **2** |
|---|---|
| Formula | $C_{63}H_{53}Cu_6FN_{18}O_2$ |
| $M_r$ | 1494.47 |
| Space group | $P\bar{1}$ |
| $a$ (Å) | 13.344(6) |
| $b$ (Å) | 16.175(8) |
| $c$ (Å) | 16.597(8) |
| $\alpha$ (°) | 91.652(6) |
| $\beta$ (°) | 105.727(6) |
| $\gamma$ (°) | 93.025(6) |
| $V$ (Å$^3$) | 3440(3) |
| $Z$ | 2 |
| $\mu$ (mm$^{-1}$) | 1.878 |
| $\rho_{calc}$ (g cm$^{-3}$) | 1.443 |
| $N_t$ | 37 037 |
| $N$ | 14 483 |
| $R_1$/w$R_2$ ($I > 2\sigma(I)$) | 0.0653/0.1654 |
| $R_1$/w$R_2$ (all data) | 0.1337/0.1897 |
| GOF | 0.817 |
| max/min $\Delta e$ (e Å$^{-3}$) | 1.194/−0.708 |

## EPR spectroscopy

X-band EPR measurements were carried out on an upgraded Bruker ER-200D spectrometer equipped with an Oxford ESR 9000 cryostat, an Anritsu MF76A frequency counter, and a Bruker 035M NMR Gaussmeter with the perpendicular mode standard cavity 4102ST.

## Computational methods

Calculations reported in this paper were performed using the geometry of **2**, and spin-unrestricted DFT as implemented in the ADF2013 package.[28] The hybrid B3LYP exchange–correlation functional was used throughout,[29–31] in conjunction with the polarized triple-zeta and double-zeta quality Slater-type basis functions on Cu and main-group atoms, respectively. All phenyl groups were replaced by hydrogens in the model structure, the geometry of which was optimised in the all-ferromagnetic $S$ = 3 state. The exchange coupling constants, $J_{ij}$, of the Heisenberg–Dirac–van Vleck (HDVV) spin Hamiltonian can be estimated using the broken-symmetry approach developed by Noodleman *et al.*[32] This method establishes the one-to-one mapping between diagonal elements of the HDVV spin Hamiltonian matrix computed in products of single-centre spin functions and the diagonal elements of the exact non-relativistic Hamiltonian matrix computed in single-determinant configurations. The configurations used correspond to the highest total spin ($|\alpha\alpha\alpha\alpha\alpha\alpha\rangle$, $M_S$ = 3) and so-called broken-symmetry (BS) states with different occupation of magnetic spin-orbitals. In this case there are 31 distinct broken-symmetry states that are permutations of $|\alpha\alpha\alpha\alpha\alpha\beta\rangle$ ($M_S$ = 2), $|\alpha\alpha\alpha\alpha\beta\beta\rangle$ ($M_S$ = 1) and $|\alpha\alpha\alpha\beta\beta\beta\rangle$ ($M_S$ = 0). The remaining 32 spin functions (there are $2^6$ = 64 in total) are simply the spin-inverted counterparts of those listed above. The energies of the broken-symmetry states were computed as single points at the optimised geometry of the ferromagnetic state. Due to the non-orthogonality of the computed HS and BS single determinants, the mapping between the diagonal elements holds only approximately.[33,34] Exchange coupling constants computed in this way within the DFT framework are typically overestimated and Ruiz and co-workers have suggested that this is because the spin-projection implied in the mapping of broken-symmetry-state energies onto the diagonal elements of the isotropic exchange Hamiltonian accounts for non-dynamical electron correlation, which is already accounted for to some extent in the UDFT-BS solutions.[35a,g] For bimetallic systems, Ruiz and co-workers have proposed an alternative expression, where the energy of the BS state is mapped directly onto the energy of the lowest spin state (*i.e.* the eigenvalue of the Heisenberg Hamiltonian rather than the diagonal element).

$$E_{HS} - E_{BS} = -J_{ij}(2S_iS_j + S_i)$$

This approach has been shown to give good agreement between the computed and experimental values of $J_{ij}$, particularly when the B3LYP functional is used.[35a–f,36] This equation has been applied to polynuclear systems within the pairwise interaction approach,[6,35g,37] notably in our previous work on

the $[\{Cu_3(\mu_3\text{-}O)(\mu\text{-}4\text{-}R\text{-}pz)_3\}_2(3,5\text{-}Ph_2\text{-}4\text{-}R'\text{-}pz)_3)]^+$ cation.[8] We therefore adopt the Ruiz protocol in this work, noting that the alternative mapping proposed by Noodleman results in $J_{ij}$ values that are larger by a factor of 2.

**Synthesis of 2.** (100 mg, 0.0497 mmol) and ferricenium hexafluorophosphate (30 mg, 0.099 mmol) were mixed in 10 mL $CH_2Cl_2$ for 24 h. The reaction mixture was filtered through a pad of Celite and MeCN was layered over the filtrate; crystals of **2** were collected after one week. X-ray quality single crystals of **2** were obtained through slow evaporation of filtrate with $Et_2O$. Crystals were also obtained when the filtrate was layered with hexane or MeCN or by slow evaporation of the filtrate. The crystal obtained when layered with MeCN has three interstitial water molecules, as seen from the elemental analysis and crystal structure. Combined crystalline yield (29 mg, 38% based on PPN[**1**]). Analysis calculated for $\mathbf{2}\cdot 3H_2O$, $C_{63}H_{59}N_{18}O_5Cu_6F$, C, 48.85; H, 3.84; N, 16.28; F, 1.23. Found: C, 48.58; H, 3.66; N, 16.12; F, 1.22. (Total fluorine in the sample was calculated by oxygen flask combustion and ion selective electrode at the Galbraith Laboratories, Inc.) IR absorptions (KBr, in $cm^{-1}$) 3432 (br), 1602 (s), 1491 (w), 1473 (s), 1426 (w), 1398 (w), 1380 (s), 1281 (m), 1180 (s), 1107 (w), 1065 (s), 991 (w), 961 (w), 912 (w), 870 (w), 794 (w), 753 (s), 694 (s), 621 (m), 434 (w). The same product, **2**, was not obtained when PPN[**1**] was reacted with $Bu_4NF$ or oxidation with Ce(IV)-reagent followed by the addition of $Bu_4NF$. Reaction with an excess of $Bu_4NF$ results in a decomposition of PPN[**1**] (indicated by the change of color from the characteristic brown/brownish-green to blue), however, the products have not yet been identified.

## Acknowledgements

L. M. and R. G. R. acknowledge financial support for this work by the National Science Foundation, USA (CHE 1213683). K. A. acknowledges support from the HCED in Iraq. R.H. and Z.T. acknowledge the Ministry of Education, Youth and Sports of the Czech Republic (project no. LO1305).

## Notes and references

1 C. Cañada-Vilalta, T. A. O'Brien, E. K. Brechin, M. Pink, E. R. Davidson and G. Christou, *Inorg. Chem.*, 2004, **43**, 5505–5521.
2 S. M. Gorun, G. C. Papaefthymiou, R. B. Frankel and S. J. Lippard, *J. Am. Chem. Soc.*, 1987, **109**, 4244–4255.
3 S. M. Gorun and S. J. Lippard, *J. Am. Chem. Soc.*, 1985, **107**, 4568–4570.
4 A. Riisio, M. M. Hanninen and R. Sillanpaa, *Eur. J. Inorg. Chem.*, 2012, 1048–1053.
5 I. Bertini, C. Luchinat and G. Parigi, *Solution NMR of paramagnetic molecules: applications to metallobiomolecules and models*, Elsevier Science, 2001.
6 E. Ruiz, *Struct. Bonding*, 2004, **113**, 71.
7 G. Mezei, M. Rivera-Carrillo and R. G. Raptis, *Dalton Trans.*, 2007, 37–40.
8 E. M. Zueva, M. M. Petrova, R. Herchel, Z. Travnicek, R. G. Raptis, L. Mathivathanan and J. E. McGrady, *Dalton Trans.*, 2009, 5924–5932.
9 (*a*) S. Wuttke, A. Lehmann, G. Scholz, M. Feist, A. Dimitrov, S. I. Troyanov and E. Kemnitz, *Dalton Trans.*, 2009, 4729–4734; (*b*) C. Knapp, E. Lork, P. G. Watson and R. Mews, *Inorg. Chem.*, 2002, **41**, 2014–2025; (*c*) F.-Q. Liu, A. Kuhn, R. Herbst-Irmer, D. Stalke and H. W. Roesky, *Angew. Chem., Int. Ed.*, 1994, **33**, 555–556.
10 (*a*) T. V. Popova and N. V. Aksenova, *Russ. J. Coord. Chem.*, 2003, **29**, 743–765; (*b*) Y. Ye, S. D. Schimler, P. S. Hanley and M. S. Sanford, *J. Am. Chem. Soc.*, 2013, **135**, 16292–16295.
11 (*a*) A. Naqui and S. D. Varfolomeev, *FEBS Lett.*, 1980, **113**, 157; (*b*) K. P. Kepp, *Inorg. Chem.*, 2015, **54**, 476–483.
12 R. Fernandez-Galan, B. R. Manzano, A. Otero, M. Lanfranchi and M. A. Pellinghelli, *Inorg. Chem.*, 1994, **33**, 2309–2312.
13 (*a*) J. Vela, J. M. Smith, Y. Yu, N. A. Ketterer, C. J. Flaschenriem, R. J. Lachicotte and P. L. Holland, *J. Am. Chem. Soc.*, 2005, **127**, 7857–7870; (*b*) D. L. Reger, R. P. Watson, J. R. Gardinier, M. D. Smith and P. J. Pellechia, *Inorg. Chem.*, 2006, **45**, 10088–10097; (*c*) B. F. Straub, F. Rominger and P. Hofmann, *Inorg. Chem.*, 2000, **39**, 2113–2119.
14 S. A. Kumalah Robinson, M.-V. L. Mempin, A. J. Cairns and K. T. Holman, *J. Am. Chem. Soc.*, 2011, **133**, 1634–1637.
15 A. Kamiyama, T. Kajiwara and T. Ito, *Chem. Lett.*, 2002, **17**, 9–12.
16 H. Zhang, Y. Lu, Z.-m. Zhang and E.-b. Wang, *Inorg. Chem. Commun.*, 2012, **17**, 9–12.
17 W. Cañon-Mancisidor, C. J. Gomez-Garcia, G. M. Espallargas, A. Vega, E. Spodine, D. Venegas-Yazigi and E. Coronado, *Chem. Sci.*, 2014, **5**, 324–332.
18 P. A. Angaridis, P. Baran, R. Boca, F. Cervantes-Lee, W. Haase, G. Mezei, R. G. Raptis and R. Werner, *Inorg. Chem.*, 2002, **41**, 2219–2228.
19 R. Boca, L. Dlhan, G. Mezei, T. Ortiz-Pérez, R. G. Raptis and J. Telser, *Inorg. Chem.*, 2003, **42**, 5801–5803.
20 E. V. Lider, E. V. Persypkina, A. I. Smolentsev, V. N. Elokhina, T. I. Yaroshenko, A. V. Virovets, V. N. Ikorskii and L. G. Lavrenova, *Polyhedron*, 2007, **26**, 1612–1618.
21 R. Boča and R. Herchel, *Coord. Chem. Rev.*, 2010, **254**, 2973–3025.
22 T. Moriya, *Phys. Rev.*, 1960, **120**, 91–98.
23 (*a*) L. Banci, A. Bencini and D. Gatteschi, *Inorg. Chem.*, 1983, **22**, 2681–2683; (*b*) I. A. Koval, H. Akhideno, S. Tanase, C. Belle, C. Duboc, E. Saint-Aman, P. Gamez, D. M. Tooke, A. L. Spek, J.-L. Pierre and J. Reedijk, *New J. Chem.*, 2007, **31**, 512–518; (*c*) M. V. Fedin, S. L. Veber, I. A. Gromov, V. I. Ovcharenko, R. Z. Sagdeev and E. G. Bagryanskaya, *J. Phys. Chem. A*, 2007, **111**, 4449–4455; (*d*) M. V. Fedin, S. L. Veber, E. L. Bagryanskaya and

 

V. I. Ovcharenko, *Coord. Chem. Rev.*, 2015, **289–290**, 341–356 and references therein.

24 (*a*) *Data collection: APEX2 suite*, Bruker AXS Inc., Madison, WI, USA, 2010; (*b*) *Data reduction and refinement: SAINT, SHELXT and SHELXL in APEX3 suite*, Bruker AXS Inc., Madison, WI, USA, 2015.

25 G. M. Sheldrick, *Acta Crystallogr., Sect. C: Cryst. Struct. Commun.*, 2015, **71**, 3–8.

26 A. L. Spek, *Acta Crystallogr., Sect. D: Biol. Crystallogr.*, 2009, **65**, 148–155.

27 R. Boča, *A Handbook of Magnetochemical Formulae*, Elsevier, Amsterdam, 2012.

28 (*a*) G. te Velde, F. M. Bickelhaupt, S. J. A. van Gisbergen, C. Fonseca Guerra, E. J. Baerends, J. G. Snijders and T. Ziegler, *J. Comput. Chem.*, 2001, **22**, 931–967; (*b*) C. Fonseca Guerra, J. G. Snijders, G. te Velde and E. J. Baerends, *Theor. Chem. Acc.*, 1998, **99**, 391–403; (*c*) ADF2013, SCM, Theoretical Chemistry, Vrije Universiteit, Amsterdam, The Netherlands, http://www.scm.com.

29 D. Becke, *J. Chem. Phys.*, 1993, **98**, 5648–5652.

30 P. J. Stevens, J. F. Devlin, C. F. Chabalowski and M. J. Frisch, *J. Phys. Chem.*, 1994, **98**, 11623–11627.

31 C. Lee, W. Yang and R. G. Parr, *Phys. Rev. B: Condens. Matter Mater. Phys.*, 1988, **37**, 785–789.

32 (*a*) L. Noodleman and J. G. Norman Jr., *J. Chem. Phys.*, 1979, **70**, 4903–4906; (*b*) L. Noodleman, *J. Chem. Phys.*, 1981, **74**, 5737–5743; (*c*) L. Noodleman and E. R. Davidson, *Chem. Phys.*, 1986, **109**, 131–143; (*d*) L. Noodleman and D. A. Case, *Adv. Inorg. Chem.*, 1992, **38**, 423–470.

33 A. Bencini and F. Totti, *Int. J. Quantum Chem.*, 2005, **101**, 819–825.

34 (*a*) R. Caballol, O. Castell, F. Illas, P. R. Moreira and J. P. Malrieu, *J. Phys. Chem. A*, 1997, **101**, 7860–7866; (*b*) T. Soda, Y. Kitagawa, T. Onishi, Y. Takano, Y. Shigeta, H. Nagao, Y. Yoshioka and K. Yamaguchi, *Chem. Phys. Lett.*, 2000, **319**, 223–230; (*c*) E. Ruiz, A. Rodriguez-Fortea, J. Cano, S. Alvarez and P. Alemany, *J. Comput. Chem.*, 2003, **24**, 982–989; (*d*) M. Shoji, K. Koizumi, Y. Kitagawa, T. Kawakami, S. Yamanaka, M. Okumura and K. Yamaguchi, *Chem. Phys. Lett.*, 2006, **432**, 343–347; (*e*) E. M. Zueva, S. A. Borshch, M. M. Petrova, H. Chermette and An. M. Kuznetsov, *Eur. J. Inorg. Chem.*, 2007, 4317–4325.

35 (*a*) E. Ruiz, J. Cano, S. Alvarez and P. Alemany, *J. Comput. Chem.*, 1999, **20**, 1391–1400; (*b*) E. Ruiz, P. Alemany, S. Alvarez and J. Cano, *J. Am. Chem. Soc.*, 1997, **119**, 1297–1303; (*c*) E. Ruiz, P. Alemany, S. Alvarez and J. Cano, *Inorg. Chem.*, 1997, **36**, 3683–3688; (*d*) E. Ruiz, J. Cano, S. Alvarez and P. Alemany, *J. Am. Chem. Soc.*, 1998, **120**, 11122–11129; (*e*) E. Ruiz, C. Graaf, P. Alemany and S. Alvarez, *J. Phys. Chem. A*, 2002, **106**, 4938–4941; (*f*) A. Rodriguez-Fortea, P. Alemany, S. Alvarez and E. Ruiz, *Eur. J. Inorg. Chem.*, 2004, 143–153; (*g*) E. Ruiz, A. Rodriguez-Fortea, J. Cano, S. Alvarez and P. Alemany, *J. Comput. Chem.*, 2003, **24**, 982–989; (*h*) E. Ruiz, A. Rodriguez-Fortea, P. Alemany and S. Alvarez, *Polyhedron*, 2001, **20**, 1323–1330; (*i*) E. Ruiz, J. Cano, S. Alvarez, A. Caneschi and D. Gatteschi, *J. Am. Chem. Soc.*, 2003, **125**, 6791–6794.

36 E. Ruiz, S. Alvarez, J. Cano and V. Polo, *J. Chem. Phys.*, 2005, **123**, 164110–164117.

37 J. Cano, R. Costa, S. Alvarez and E. Ruiz, *J. Chem. Theory Comput.*, 2007, **3**, 782–788.